Theses and Dissertations   1. Thesis and Dissertation Collection, all items

2006-12

Imaging of 3.4 THz quantum cascade laser beam using uncooled microbolometer camera

Lowe, Michele N

Monterey California. Naval Postgraduate School

https://hdl.handle.net/10945/2463

NAVAL
POSTGRADUATE
SCHOOL

MONTEREY, CALIFORNIA

THESIS

IMAGING OF 3.4 THz QUANTUM CASCADE LASER
BEAM USING AN UNCOOLED MICROBOLOMETER CAMERA

by

Michele Lowe

December 2006

Thesis Advisor: Gamani Karunasiri
Second Reader: Nancy Haegel

Approved for public release; distribution is unlimited

THIS PAGE INTENTIONALLY LEFT BLANK

REPORT DOCUMENTATION PAGE		*Form Approved OMB No. 0704-0188*
Public reporting burden for this collection of information is estimated to average 1 hour per response, including the time for reviewing instruction, searching existing data sources, gathering and maintaining the data needed, and completing and reviewing the collection of information. Send comments regarding this burden estimate or any other aspect of this collection of information, including suggestions for reducing this burden, to Washington headquarters Services, Directorate for Information Operations and Reports, 1215 Jefferson Davis Highway, Suite 1204, Arlington, VA 22202-4302, and to the Office of Management and Budget, Paperwork Reduction Project (0704-0188) Washington DC 20503.		
1. AGENCY USE ONLY *(Leave blank)*	**2. REPORT DATE** December 2006	**3. REPORT TYPE AND DATES COVERED** Master's of Science
4. TITLE AND SUBTITLE Imaging of 3.4 THz Quantum Cascade Laser Beam using Uncooled Microbolometer Camera		**5. FUNDING NUMBERS**
6. AUTHOR(S) Michele Lowe		
7. PERFORMING ORGANIZATION NAME(S) AND ADDRESS(ES) Naval Postgraduate School Monterey, CA 93943-5000		**8. PERFORMING ORGANIZATION REPORT NUMBER**
9. SPONSORING /MONITORING AGENCY NAME(S) AND ADDRESS(ES) N/A		**10. SPONSORING/MONITORING AGENCY REPORT NUMBER**
11. SUPPLEMENTARY NOTES The views expressed in this thesis are those of the author and do not reflect the official policy or position of the Department of Defense or the U.S. Government.		
12a. DISTRIBUTION / AVAILABILITY STATEMENT Approved for public release; distribution is unlimited		**12b. DISTRIBUTION CODE**

13. ABSTRACT (maximum 200 words)

The employment of terahertz (THz) technology for applications including Improvised Explosive Device (IED) and concealed weapons detection is a rapidly growing field of research. Additionally, THz waves do not pose a health hazard as do x-rays and as such can be used for the imaging and detection of certain cancers. To date, however, most detectors are highly sophisticated, bulky systems which require extensive cooling in order to provide a signal-to-noise (SNR) ratio high enough for detection. A detection system that is simple in operation and uncooled is highly desirable and is the focus of this research.

In this thesis, operation of a 3.4 THz quantum cascade laser (QCL) was successfully achieved using a closed cycle cryostat and nanosecond pulse generator with impedance matching circuitry. The laser beam was imaged in real time using an uncooled microbolometer infrared camera typically used in far-infrared wavelength band (8-12 µm). The preliminary findings offer potential for development of a compact THz imaging system for applications involving concealed object detection.

14. SUBJECT TERMS Terahertz, Quantum Cascade Laser, Microbolometer, Uncooled Detector			**15. NUMBER OF PAGES** 63
			16. PRICE CODE
17. SECURITY CLASSIFICATION OF REPORT Unclassified	**18. SECURITY CLASSIFICATION OF THIS PAGE** Unclassified	**19. SECURITY CLASSIFICATION OF ABSTRACT** Unclassified	**20. LIMITATION OF ABSTRACT** UL

NSN 7540-01-280-5500

Standard Form 298 (Rev. 2-89)
Prescribed by ANSI Std. 239-18

THIS PAGE INTENTIONALLY LEFT BLANK

Approved for public release; distribution is unlimited

IMAGING OF 3.4 THz QUANTUM CASCADE LASER BEAM USING AN UNCOOLED MICROBOLOMETER CAMERA

Michele N. Lowe
Lieutenant, United States Navy
B.A., University of Florida, 2000

Submitted in partial fulfillment of the
requirements for the degree of

MASTER OF SCIENCE IN APPLIED PHYSICS

from the

NAVAL POSTGRADUATE SCHOOL
December 2006

Author: Michele Lowe

Approved by: Gamani Karunasiri
                 Thesis Advisor

                 Nancy Haegel
                 Second Reader

                 James H. Luscombe
                 Chairman, Department of Physics

THIS PAGE INTENTIONALLY LEFT BLANK

ABSTRACT

The employment of terahertz (THz) technology for applications including Improvised Explosive Device (IED) and concealed weapons detection is a rapidly growing field of research. Additionally, THz waves do not pose a health hazard as do x-rays and as such can be used for the imaging and detection of certain cancers. To date, however, most detectors are highly sophisticated, bulky systems which require extensive cooling in order to provide a signal-to-noise (SNR) ratio high enough for detection. A detection system that is simple in operation and uncooled is highly desirable and is the focus of this research.

In this thesis, operation of a 3.4 THz quantum cascade laser (QCL) was successfully achieved using a closed cycle cryostat and nanosecond pulse generator with impedance matching circuitry. The laser beam was imaged in real time using an uncooled microbolometer infrared camera typically used in far-infrared wavelength band (8-12 μm). The preliminary findings offer potential for development of a compact THz imaging system for applications involving concealed object detection.

THIS PAGE INTENTIONALLY LEFT BLANK

TABLE OF CONTENTS

THIS PAGE INTENTIONALLY LEFT BLANK

LIST OF FIGURES

LIST OF TABLES

THIS PAGE INTENTIONALLY LEFT BLANK

ACKNOWLEDGMENTS

even when experiments did not yield results. My research would have been impossible without his leadership and I am forever grateful for the impact he has had on my life.

I would like to thank my support at home, John. It was only with his love, sacrifice, patience, and support that I was able to get through this incredible challenge.

I.   INTRODUCTION

A.   TERAHERTZ IMAGING

Imaging using terahertz (THz) frequencies has recently gained momentum due to its penetration through non-conducting materials [1-2]. The advances in detection devices and increase in convenient high power emitters as well as fabrication of adaptive optics makes this region available for imaging. These waves are short enough for submillimeter imaging while long enough to penetrate many materials [3]. This characteristic property makes THz imaging a promising solution to detecting Improvised Explosive Devices (IEDs) and concealed weapons for airport security as the technology matures.

Additionally, THz waves produce no health threats like x-ray radiation. Most of the energy present in these waves is dissipated through the first 100 mm of the skin [4-5]. Deeper penetration is not possible due to water content. These waves do not contain enough energy to affect the underlining organs which makes THz imaging ideal for medical purposes.

B.   TERAHERTZ WAVES

The terahertz region of the electromagnetic spectrum ranges from 300 GHz to 10 THz corresponding to wavelengths of 30 μm to 1000 μm. These wavelengths fall into what is called the far-infrared or submillimeter wave region, commonly referred to as submillimeter-terahertz (SMM-THz) [6]. The characteristics of wavelengths in this region

allow submillimeter resolution while containing enough
energy to penetrate through many materials. Figure 1 shows
where the THz region lies in the frequency spectrum.
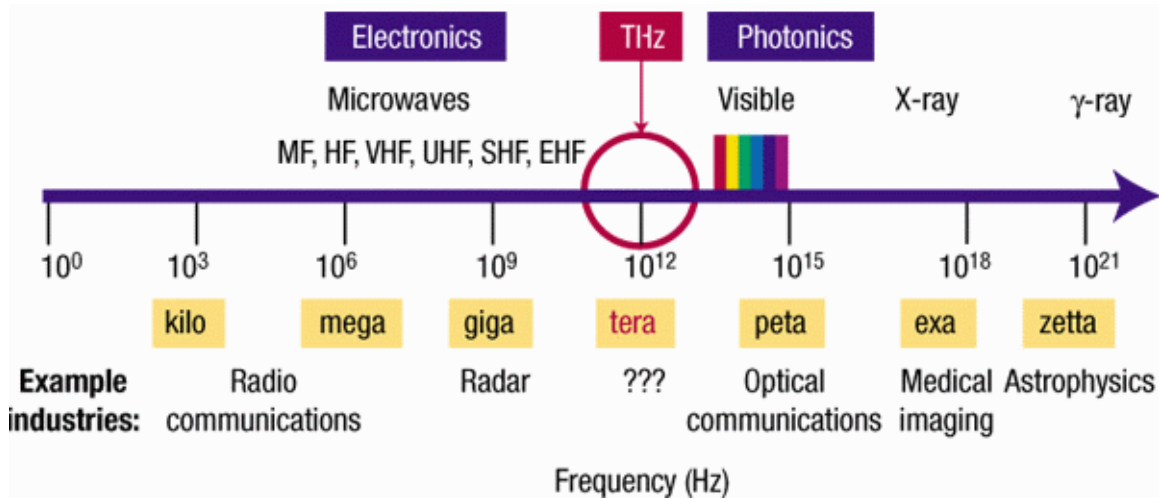
Figure 1.   Frequency Spectrum (From [7]).

The energy of THz photons ranges from about 0.001 to
0.04 eV. This range is comparable with thermal energy at
room temperature (300 K) which has a value of 0.026 eV. In
order to detect thermally generated THz radiation, highly
sensitive detection schemes are needed to overcome the
thermal noise generated by the environment. In other
words, THz radiation is nearly impossible to pick out from
all the background thermal energy radiating at all
frequencies.

C.   TERAHERTZ SOURCES

To date, several THz sources are available for imaging
applications using external illumination [8-10]. These
include photomixer technologies, Schottky multipliers, free
electron lasers and quantum cascade lasers. Photomixers
with a femtosecond pulsed laser illuminate low temperature-

grown gallium arsenide (GaAs) but can only generate broadband THz radiation [9]. Free electron lasers provide wavelength tenability but require large, bulky equipment [10]. Quantum cascade lasers (QCL) emit coherent THz radiation at a narrow bandwidth but need significant cooling in order to lase. The various approaches in generating THz radiation are summarized in Figure 2 [8]. This research uses QCLs to generate THz radiation.
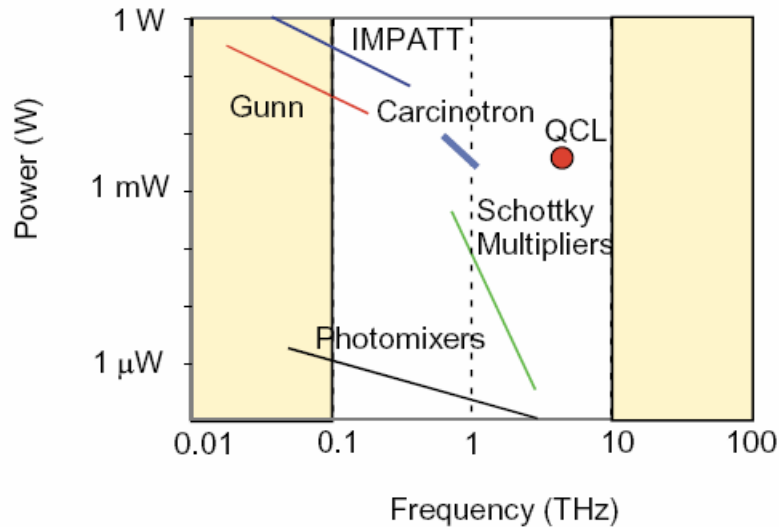
Figure 2.   Approaches used to generate THz radiation
(From [8]).

D.   TERAHERTZ DETECTORS

Detectors designed specifically for imaging in THz have already been demonstrated. Typically these systems are expensive and in some cases require cooling to below 77K. In order to apply THz imaging to everyday life, detectors must become portable, easier to use, cheaper, and uncooled. As semiconductor technology improves, a system capable of achieving all these milestones now exists. Uncooled microbolometers are already being fabricated for

near and mid-infrared imaging [11]. This research demonstrates the ability of an uncooled microbolometer with THz compatible optics to image THz radiation.

II. THEORETICAL BACKGROUND

The aim of the following sections is to derive an expression for the Noise Equivalent Temperature Difference (NETD) for the uncooled camera in THz wavelengths. This analysis requires the total background THz power as a function of the cut-off frequency. The NETD analysis was not completed due to time constraints associated with making the laser operational.

A. BLACKBODY RADIATION

A blackbody is any piece of matter which absorbs all wavelengths of light, thus making it appear completely black. The thermal radiation emitted by such an object is known as "blackbody radiation." This radiation obeys Planck's radiation law [12] and can be written in terms of frequency and temperature as follows:

$$P(\boldsymbol{n},T) = \frac{2\boldsymbol{p}h\boldsymbol{n}^3}{c^2} \frac{1}{e^{h\boldsymbol{n}/kT} - 1} \, ,$$ (2.1)

where h is the Planck constant (6.64×10^{-34} Js), $\boldsymbol{n}$ is the frequency of radiated light, c is the speed of light in a vacuum (3×10^8 m/s), k is the Boltzmann constant (1.38×10^{-23} J/K), and T is the temperature in Kelvin. Equation 2.1 can be simplified by observing that photon energies up to 5 THz (0.021 eV) are less than kT at room temperature (0.026 eV):

$$hv = (6.63 x 10^{-34} Js)(3.4 x 10^{12} Hz) = 2.45 x 10^{-21} J$$
$$hv < kT$$

Applying a Taylor expansion to the exponential in Equation 2.1 gives:

exp(hv/kT) -1 ~ hv/kT

where higher order terms contribute little to the overall value of the equation and are consequently dropped. Equation 2.1 then becomes:

$$P(\mathbf{n}, T) = \frac{2\mathbf{p}kT\mathbf{n}^2}{c^2} .$$

(2.2)

Equation 2.2 gives the power emitted per unit area per unit frequency interval. In order to get the total THz power per unit area, frequency is taken out of the equation by integrating over the THz frequency domain $(0, \mathbf{v}_c)$:

$$P(T) = \int_0^{\mathbf{n}_c} \frac{2\mathbf{p}kT\mathbf{n}^2}{c^2} d\mathbf{n} = \frac{2\mathbf{p}kT}{3c^2}\mathbf{n}_c^3 .$$

(2.3)

Using the approximation given by equation 2.3 allows the exitance to be easily calculated and graphed in Figure (3).

x 10⁻¹² Power Emitted Per Unit Area Per Unit Frequency Interval
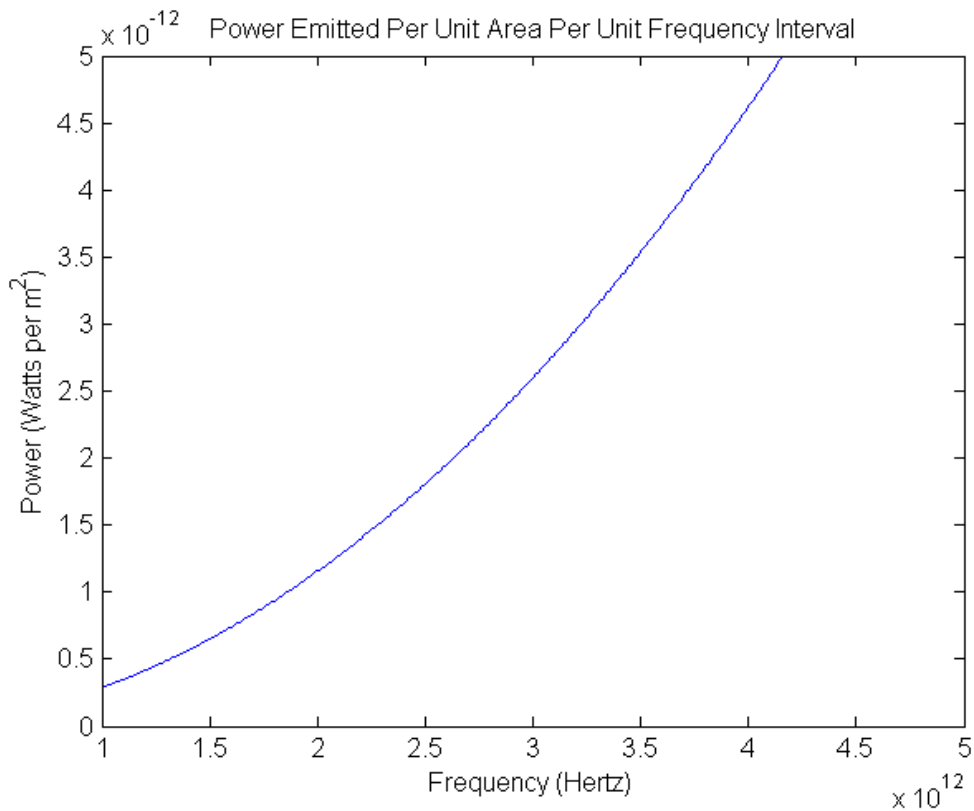
Figure 3.   Power emitted as a function of THz frequency using Equation 2.3 at 300K.

6

Before accepting data provided from the approximation above, the actual value of P(T) is calculated by numerically integrating equation 2.1 over the same frequency domain as follows:

$$P(T) = d\mathbf{n} \sum_{\mathbf{n}=5d\,2} \frac{2\mathbf{p}h\mathbf{n}^3}{c^2} \frac{1}{e^{h\mathbf{n}/kT} - 1} \, . \qquad (2.4)$$

where $d\mathbf{n}$ was taken to be $1\mathrm{x}10^8$ Hz. The results of equation 2.4 are depicted in Figure 4.
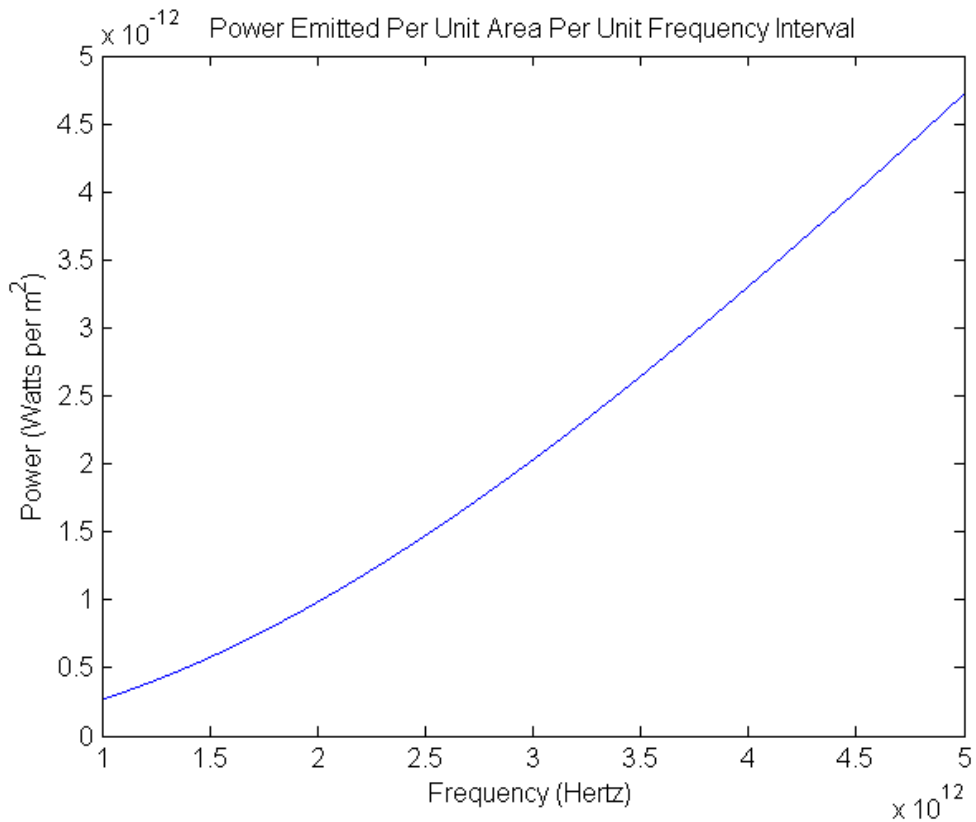
Figure 4.   Power emitted as a function of THz frequency using Equation 2.4 at 300K.
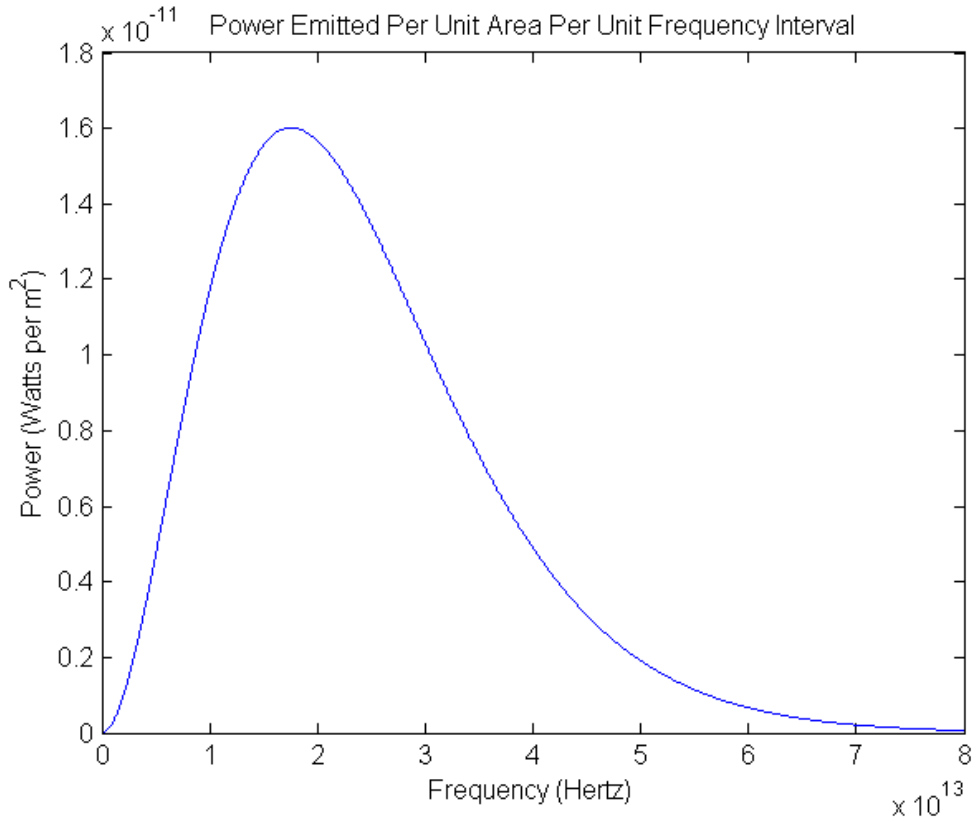
Figure 5.   Blackbody radiation exitance as a function
of frequency at 300K.

Next, equations 2.3 and 2.4 are graphed together with power on the vertical axis and temperature on the horizontal axis in order to determine whether the approximation agrees:
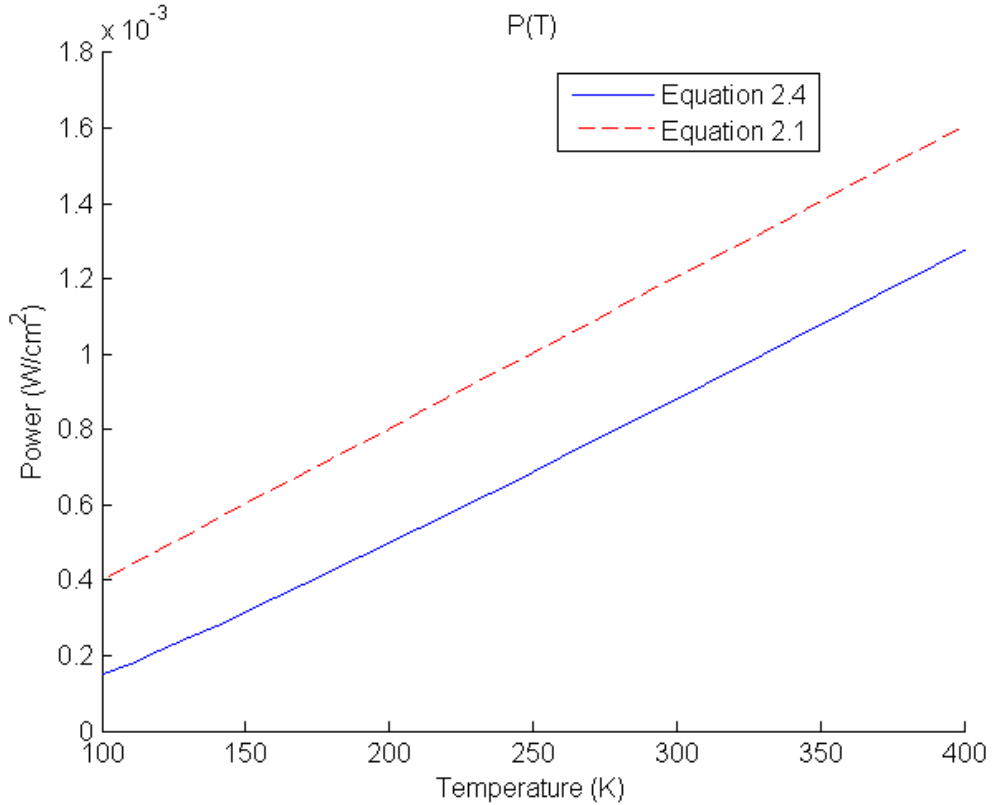
Figure 6.   Comparison of power emitted using Equations
2.3 and 2.4.

It is easily seen in Figure 6 that the estimated power
using the two equations at 300 K are approximately the
same.

It has been determined above that equations 2.3 and
2.4 yield approximately the same result at room temperature
and above. Figure 5 shows the blackbody radiation curve at
300K. Using equation 2.4, the area under the curve is
found by summing all the P(T)s and multiplying by a small
step, $d\nu$ =1x10^8 Hz. The area under the curve is found to be:

$$P(T) = 45.7\,{mW}\!\!\Big/\!\!{cm^2}\;.$$

9

The numerical integration can be verified using the Stefan-Boltzmann law [13]:

$$P(T) = \boldsymbol{s} T^4 \tag{2.5}$$

The total energy radiated per unit surface area for a blackbody is calculated using equation 2.5. At 300K (background temperature), equation 2.6 gives:

$$P(T) = 45.9 \, mW \Big/ cm^2$$

The two values from equations 2.4 and 2.5 agree to within one percent. The value yielded demonstrates that the terahertz power in the 1-5 THz range is much weaker compared to the total background radiation power, making passive detection nearly impossible using uncooled thermal sensors. However, passive detection has been achieved using liquid helium cooled superconducting microbolometer sensors [24]. Therefore, for an uncooled thermal sensor, an external THz source is needed to enhance the signal-to-noise ratio. This research uses a quantum cascade laser and uncooled microbolometer for these purposes. Both are discussed in detail in the following sections.

B.   MICROBOLOMETER OPERATION

This research utilizes an uncooled, silicon nitride and vanadium oxide (VO_x) microbolometer camera, the IR-160 Thermal Imager, in THz imaging. Its original wavelength band is 8-14 $\boldsymbol{m}m$ (infrared). It has a 160x120 pixel focal plane array and a sensitivity of under 60mK with its f/1 germanium lens [15].

Figure 7.   IR-160 Thermal Imager (From [15]).

The structure of the microbolometer pixel consists of a silicon nitride and VO_x layer suspended over and connected to the substrate by two narrow legs. The legs serve to reduce thermal conductance (see Figure 8).   The microbolometer senses minute temperature changes through two resistors of different resistance. Radiation incident on the detector causes a temperature increase.   This temperature change causes a change in the electrical resistance of the VO_x film, which is measured by an external circuit.
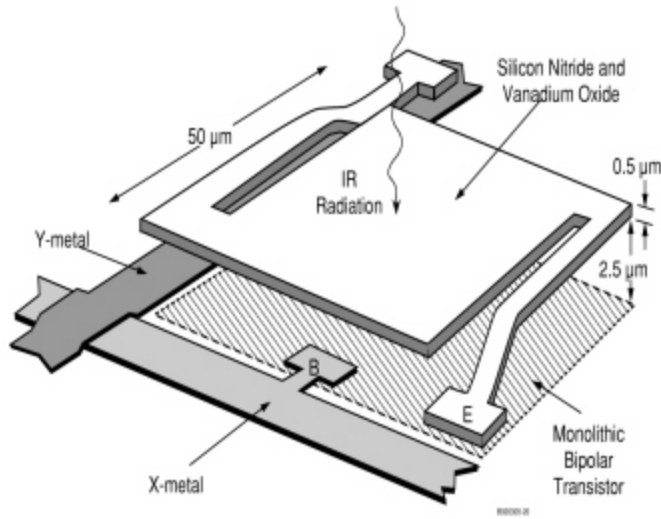
Figure 8.   Microbolometer pixel structure (From [14]).

A microbolometer's thermal sensor can be understood using Figure 9.
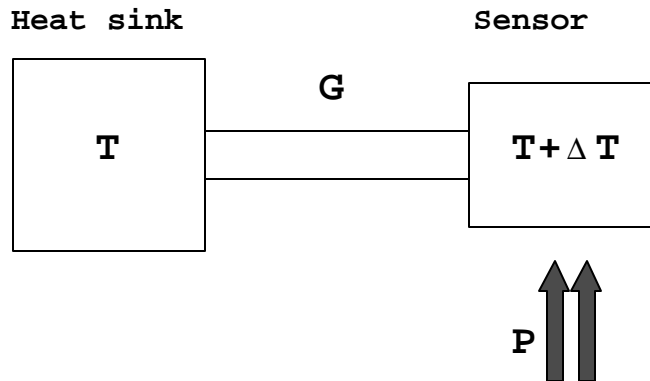
Figure 9.   Thermal sensor operation diagram.

In this diagram, the sensor is connected to a heat sink through a narrow arm.   The sensor is exposed to the environment and infrared is incident on it.   The temperature on the sensor increases and the incident power is dissipated through the narrow arm into the heat sink. The heat transfer for this system is given by:

$$P = \frac{d}{dt}C(\Delta T + T) + G\Delta T \; , \qquad (2.6)$$

12

where P is the incident power provided by an infrared source, C is the heat capacity of the sensor, ΔT is the temperature change, T is the ambient temperature, and G is the heat conductance. In the steady state case, there is no temperature change, i.e., $\frac{d}{dt}(\Delta T+T)=0$, and equation 2.6 becomes:

$$\Delta T = \frac{P}{G}. \tag{2.7}$$

For systems designed to sense temperature changes, it is desired to have a large ΔT. It is evident from equation 2.7 that this is accomplished by reducing G and making the arm between the heat sink and sensor as narrow and long as possible. This "solution" has a considerable tradeoff which is analyzed next.

The next case to analyze is when the light (P) incident on the sensor is turned off. Equation 2.6 becomes:

$$\frac{d}{dt}(C\Delta T)+G\Delta T =0. \tag{2.8}$$

Equation 2.8 is rearranged and solved for ΔT:

$$\frac{d\Delta T}{\Delta T}=-\frac{G}{C}dt, \tag{2.9}$$

$$\Delta T = \Delta T_{ss}e^{-t/C_G} = \Delta T_{ss}e^{-t/t}, \tag{2.10}$$

where $t=\frac{C}{G}$ is the response time of the bolometer and Tss is the value of ΔT at $t=0$. Fast response times are desired in detectors. This is generally not possible because as mentioned earlier equation 2.7 requires a small G; however, equation 2.10 explicitly shows that smaller G

13

slows the detector's response time. Therefore, G is maximized to provide the best ΔT while providing the fastest possible response time. The microbolometer pixels used in this research have a response time of $t \cong 12ms$ [15].

The final condition to analyze is when the incident power is time dependent, $P = P_o e^{jwt}$. Equation 2.6 becomes:

$$P_o e^{jwt} = C\frac{d\Delta T}{dt} + G\Delta T .$$ (2.11)

The steady state solution to this equation is given by [12]:

$$\Delta T = \frac{P_o e^{jwt}}{\sqrt{G^2 + w^2 C^2} e^{jq}} = \frac{P_o e^{j(wt-q)}}{G(1 + w^2 t^2)^{\frac{1}{2}}} .$$ (2.12)

where the e^{-jq} term is the phase lag of ΔT behind P_o. As the frequency is increased, the phase lag continues to decrease. The amount of temperature change as a function of temperature is given by:

$$|\Delta T| = \frac{P_o}{G(1 + w^2 t^2)^{1/2}} .$$ (2.13)

As a function of frequency, $|\Delta T|$ rolls off with a 3 dB cutoff frequency at $1/(2\pi\tau)$. A typical microbolometer detector (with thermal time constant of about 5 ms) gives a cutoff frequency of about 30 Hz.

C. QUANTUM CASCADE LASER

In this research, a 3.4 THz quantum cascade laser (QCL) was used. Specifically, the laser was a bound-to-continuum design fabricated by the Jerome Faist group at the University of Neuchatel, Switzerland and was provided to us by Danielle Chamberlin and Peter Robrish at Agilent

14

Laboratories in Santa Clara. QCLs are constructed so that
the active region is layered with several thin-layer
materials [17-18].

1.   Solid-state Diode Laser Compared to QC Laser

Figure 10 shows the layer structure and operation
contrast between a quantum well based diode and QCL [16].
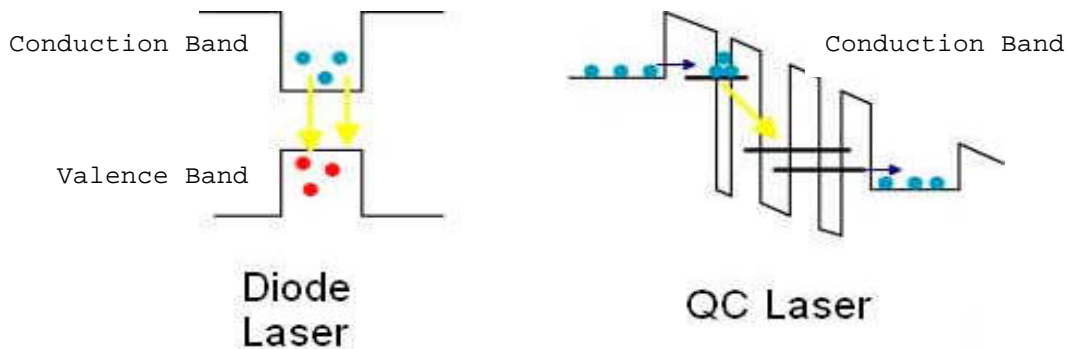
Figure 10.   Operation of a diode and QC laser (After
[16]).

Diode lasers have only one material in the active region
which effectively splits the available energy into valence
bands heavily populated by holes and conduction bands
populated with electrons. Such a population inversion is
achieved either by electrical or optical pumping [17]. A
photon is then introduced with the specific energy of the
bandgap and an electron from the conduction band is dropped
to the valence band creating a photon which is identical to
the incident photon (stimulated emission).   This process
continues to produce an amplified light beam from the
diode.

In a quantum cascade laser, the aforementioned layers
create three subbands within the conduction band as seen in
Figure 11 under an external bias.   The upper subband is

15

injected with electrons and subbands between adjacent
active regions are aligned during operation as illustrated
in Figure 11.   In this case, one electron can tunnel
through the adjacent active regions creating a photon each
time it travels through them.   The advantage in using a QCL
is one electron can emit several photons and increase the
optical output power many times over compared to the diode
laser.

The energy separation between the first two energy
states in an active region is usually made to be resonant
with optical phonon energy to enhance the depopulation
rate.   This reduces the pumping current needed to maintain
the population inversion between the 2nd and 3rd states of
each active region.
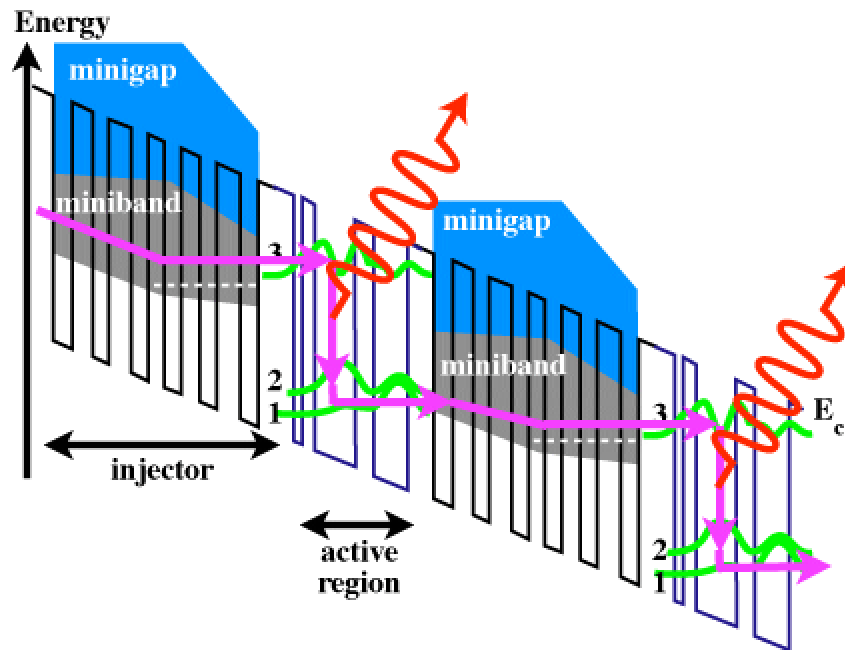
Figure 11.   Conduction band structure for QCL (After
[19]).

2. 3.4 THz QCL Operation

Experiments in this research were made using a 3.4 THz laser with a 200mm by 14mm active region as seen in Figure 12. The laser operates at high currents and voltages to overcome the relatively small non-radiative lifetime (~1 ps) for achieving population inversion. It has a substrate of semi-insulating (SI) Gallium-Arsenide (SI-GaAs), followed by a layer of n-doped GaAs. In the area labeled "MQW" in Figure 12, over 100 layers of GaAs and AlGaAs are present to create a multiple quantum well active region. The details of the design can be found in Ref. [20].

Figure 12.   Schematic of 3.4 THz laser (After [20]).

Due to the small energy level separations involved, THz QCLs usually operate in pulsed mode with temperatures below 50 K. The typical electrical pulses used are several hundreds of nanoseconds wide with a duty cycle of less than 10%, to avoid excessive heating of the active region. One of the most important parameters is the impedance of the laser under operating conditions. This is obtained using

the low temperature I-V characteristics of the laser. The details of the I-V measurement will be presented in the next chapter.

III. EXPERIMENTAL SET-UP

A. LASER HOLDER

The laser holder used in this research was designed by Agilent Laboratories.   It is made of copper, which transfers heat quickly from the laser.   Exact replication was essential to fit the QCL, a parabolic mirror, and flat mirror so that the optics maximize the power output QCL beam.   Figure 13 depicts the laser holder and Figure 14 shows a size comparison for the laser, laser holder with parabolic mirror compared to a quarter.
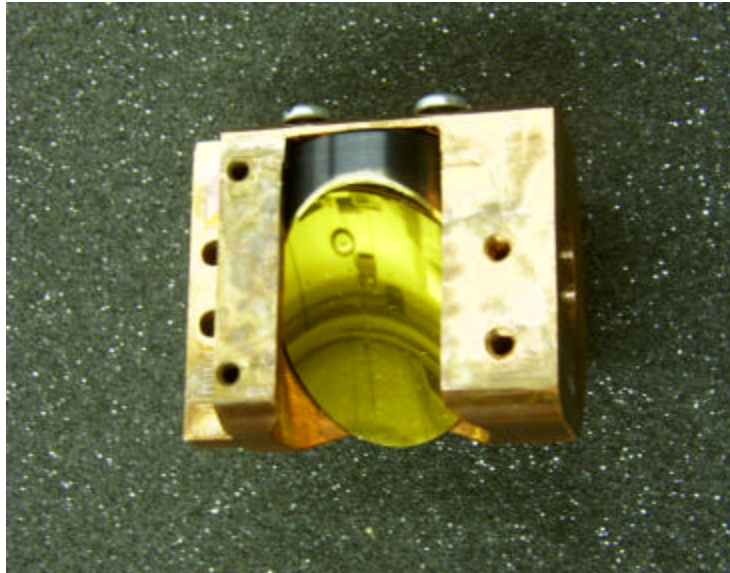
Figure 13.   Laser holder with parabolic mirror.
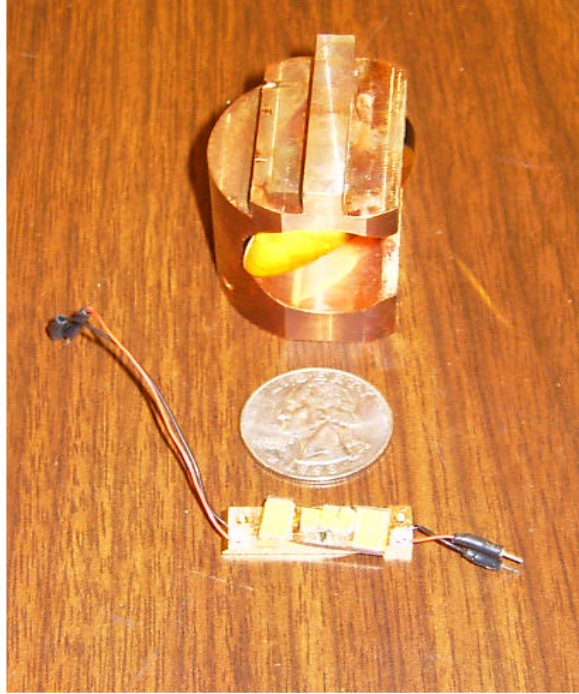
Figure 14.   Laser and laser holder size comparison with quarter.

B.   OPTICS

The optics designed for the laser holder included an 8mm x 8mm flat, gold plated mirror and a 90° off-axis, 1 inch diameter, parabolic mirror, also gold plated. The parabolic mirror was attached to the laser holder with two screws. The flat mirror was attached to the holder with epoxy. Figures 15 and 16 depict the optics layout and resulting beam from the laser.
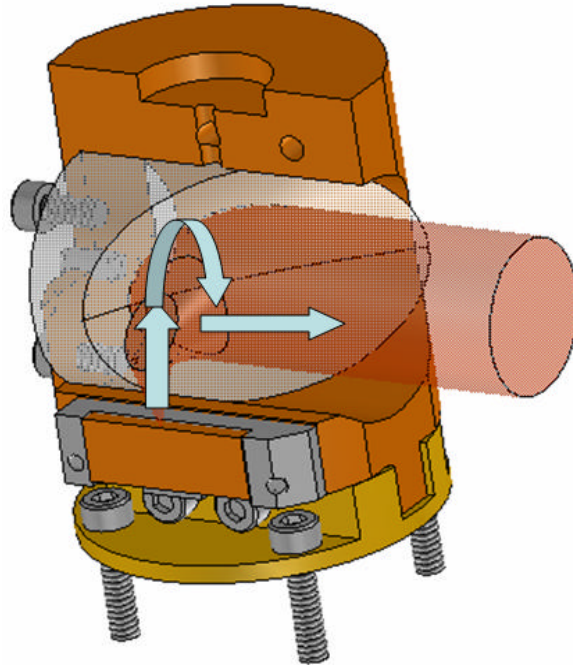
Figure 15.   Laser holder with QCL and optics. Arrows
show laser beam path (After [20]).
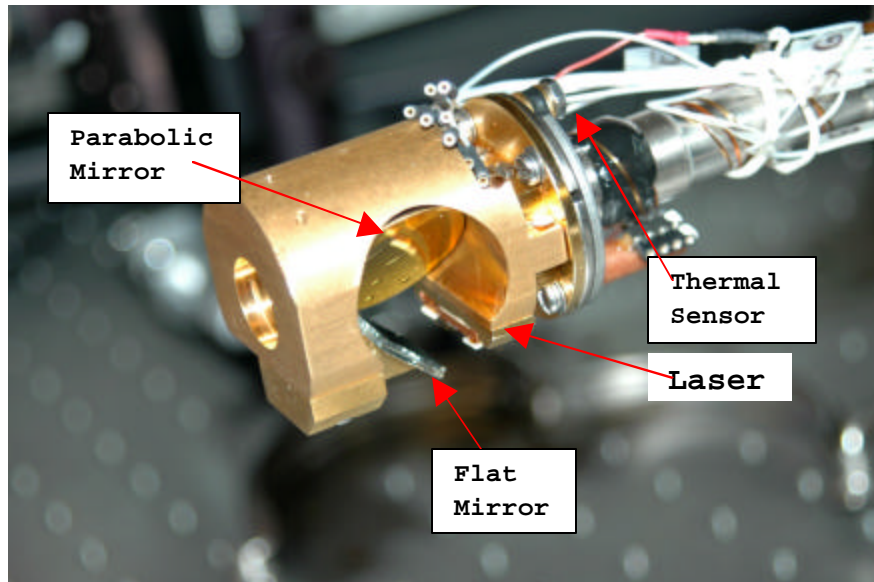
Figure 16.   Laser holder with optics mounted.

C.   QCL

The QCL described in Chapter II was mounted first on a metal strip and then onto the laser holder using two small screws. It was then connected to ground and power wires were attached to the laser holder as shown in Figure 16.

The metal strip contains two lasers which can be distinguished in Figure 18. The smaller one is 100$\textit{mm}$ wide by 14$\textit{mm}$ deep and the larger one, which was actually used in the experiments, is 200$\textit{mm}$ wide by 14$\textit{mm}$ deep (see Figure 18).
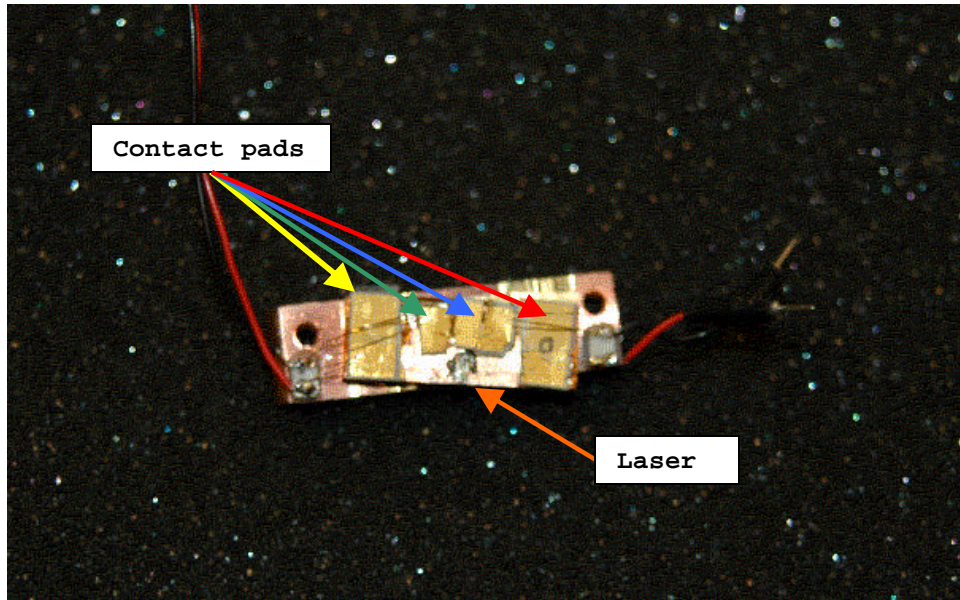
Figure 17.   3.4 THz Laser, pads, and metal holder.
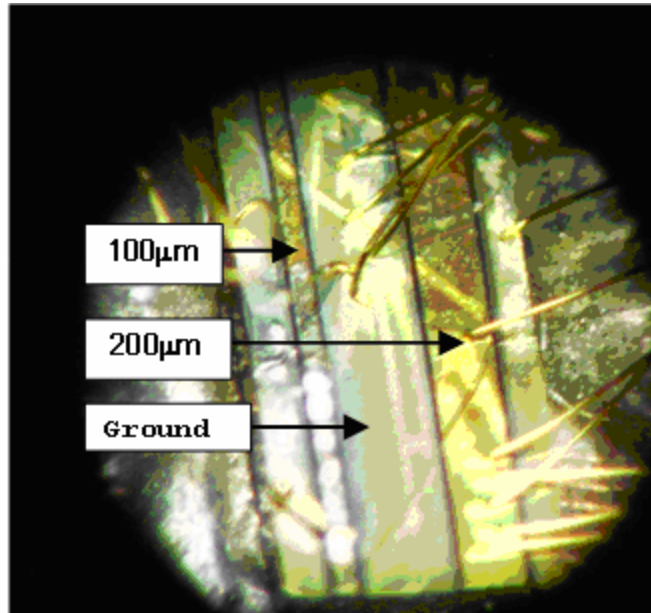
Figure 18.   Close-up of the laser.

D.   LASER COOLING SETUP

A closed-cycle refrigerator (seen in Figure 19) from Janis was used to cool the laser system to 10K.   The cryodyne system uses helium as refrigerant; evacuating air from the chamber surrounding the cold head (where the laser is housed) is needed before operation [21].

Immediately behind the laser holder connection to the cooler is the thermal sensor (see Figure 16).   The system requires approximately two hours to cool down before operation of the laser can commence.   The system temperature is continuously monitored at the LakeShore 321 Autotuning Temperature Controller (Figure 20).
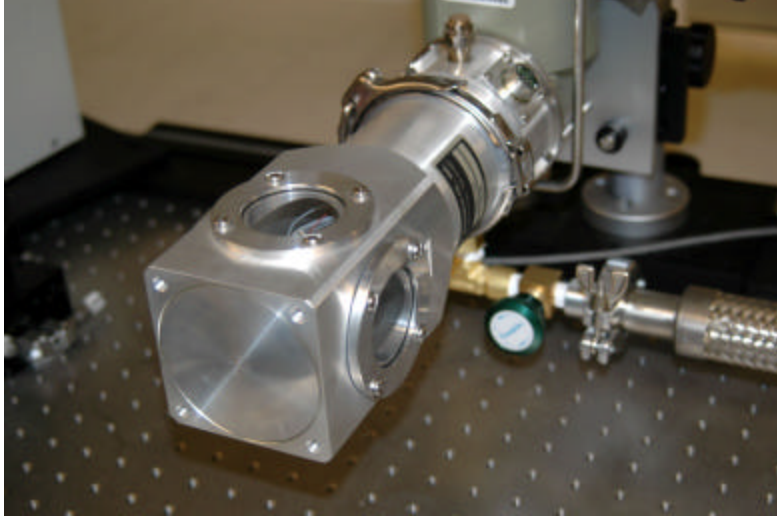
Figure 19.   Closed cycle refrigerator head where laser
is housed.

Figure 20.   LakeShore 312 Autotuning Temperature
Controller set to 10K.

E.   PICARIN WINDOW AND CAMERA LENS

A picarin window and camera lens was used in this
research because of the high THz frequency transmission.
Using a Fourier transform infrared spectrometer (FTIR), the
picarin window was analyzed to determine its transmission
compared to the manufacture's specifications. Figures 21
and 22 compare the two transmission spectra and show good
agreement. Figure 23 depicts the picarin lens used on the
microbolometer camera for imaging the THz beam from the
laser.

24
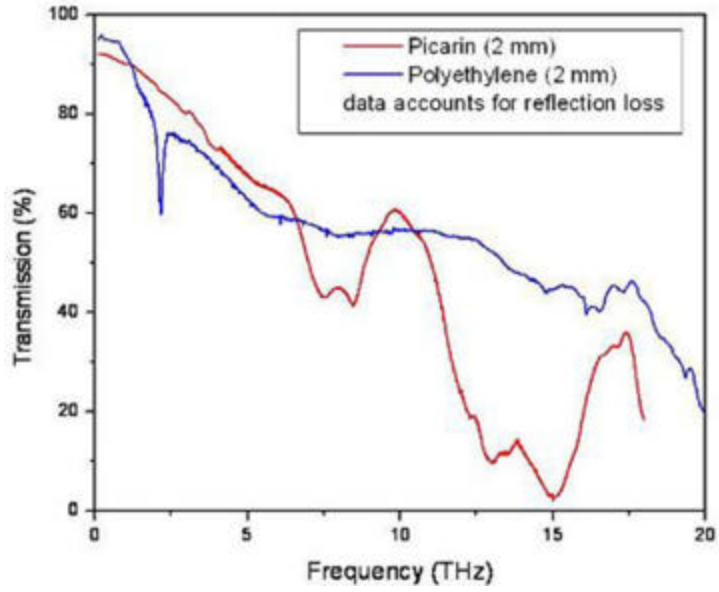
Figure 21.   Manufacturer's data depicting percent THz transmitted through picarin window. (From [18])
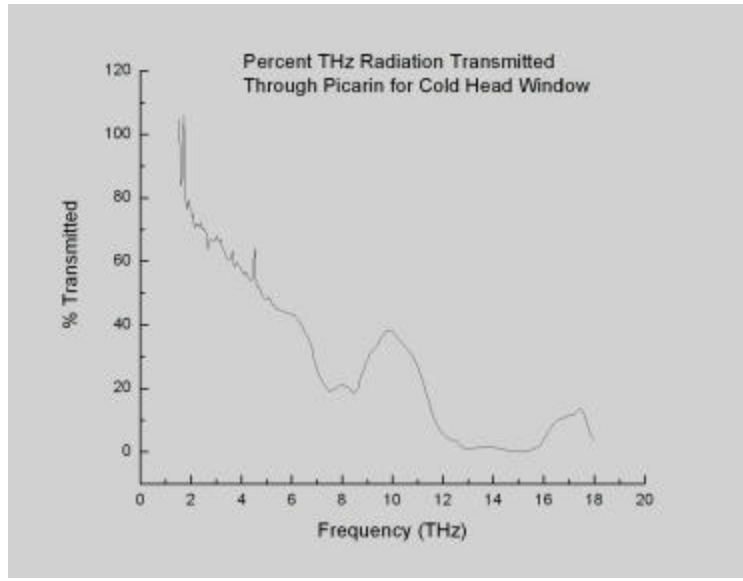
Figure 22.   THz transmission through picarin measured with FTIR.

Figure 23.   Picarin lens used for the microbolometer camera.

D.   PULSED POWER TO THE LASER

The operation of the laser requires electrical pulses of about 500 ns wide with a 100 kHz repetition rate. The QCLis a monopolar device and has about 3.47Ω impedance at its operating point as given in Reference [20]. The pulse generator and the cables have impedance of 50 Ω and require impedance matching to deliver the high current pulses to the laser. This was achieved by fabricating a step-down transformer. By selecting the number of turns of primary and secondary coils, the two impedances were matched as shown below. The transfer characteristics of the transformer give:

$$V_{in} = I_{in}Z_{in} \tag{3.1}$$

$$V_{out} = I_{out}Z_{out} \tag{3.2}$$

$$V_{in}I_{in} = V_{out}I_{out} \tag{3.3}$$

$$I_{in}N_{in} = I_{out}N_{out} \qquad\qquad (3.4)$$

$$\frac{I_{in}}{I_{out}} = \frac{N_{out}}{N_{in}} \qquad\qquad (3.5)$$

where Z_{in} is the input impedance of 50Ω, Z_{out} is the laser impedance of 3.47Ω, V is voltage, I is current, and N is the number of turns on the transformer. Next, equations 3.1 and 3.2 are substituted into equation 3.3 for V:

$$(Z_{in}I_{in})I_{in} = (Z_{out}I_{out})I_{out} \qquad\qquad (3.6)$$

$$Z_{in}I_{in}^2 = Z_{out}I_{out}^2 \; . \qquad\qquad (3.7)$$

Equation 3.7 is solved for Z_{out}:

$$Z_{out} = Z_{in}(\frac{I_{in}}{I_{out}})^2 \; . \qquad\qquad (3.8)$$

Finally, equation 3.8 is modified to include the number of turns:

$$Z_{out} = Z_{in}(\frac{N_{out}}{N_{in}})^2 \; . \qquad\qquad (3.9)$$

Plugging in the appropriate numbers for Z yields a squared turn ratio of $(\frac{N_{out}}{N_{in}})^2$ to be approximately 0.26. For this experiment, a transformer from a computer power supply with slight modifications to the number of turns to the secondary coil was used. Appendix B describes the procedure and data (Table 2) used to construct the correct turn ratio.

F.   STEP-DOWN TRANSFORMER

The above analysis yielded a squared ratio of turns equal to 0.28 to match the impedances. This translates into approximately a 2:1 ratio of voltage and 1:2 ratio of

current.   The input voltage was twice as large as the
output voltage and the input current was half as large as
the output current.   The current through the laser was
measured with a Pearson Current Monitor [23].

     The current monitor measures the change in flux of the
magnetic field and converts it to a voltage.   Using the
conversion factor specific to the monitor of 0.1V=1A, the
output current is easily measured.   Figure 24 depicts the
transformer as well as the current measurement device.
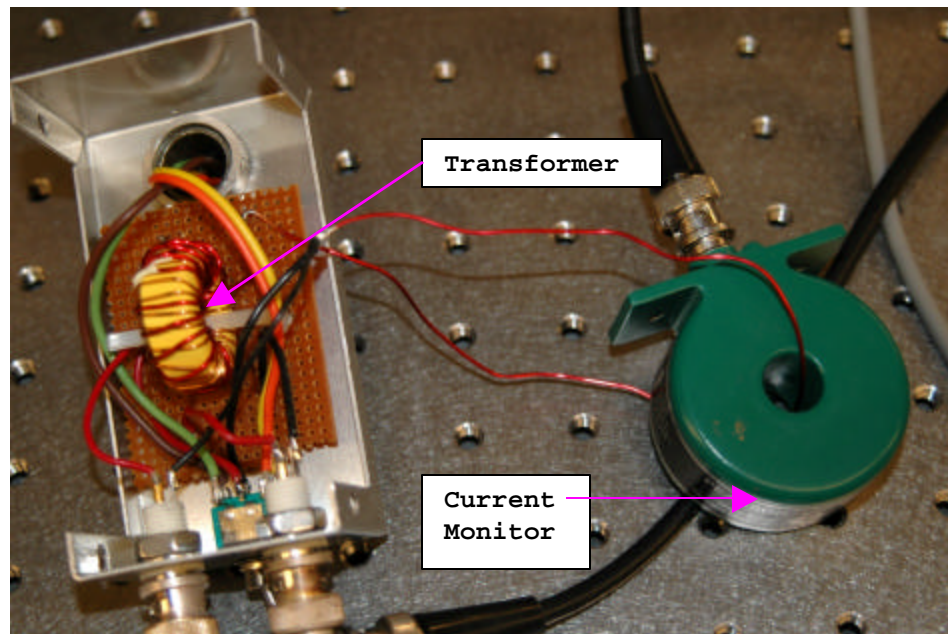
Figure 24.   Transformer and current monitor.

G.   PULSE GENERATOR AND OSCILLISCOPE

     The pulse generator used in this experiment was an
Agilent 8114A 100V/2A Programmable Pulse Generator, which
is depicted in Figure 25.   The oscilloscope used to monitor
the input and output pulses was the Agilent Infiniium
Oscilloscope as shown in Figure 26.

Figure 25.   Pulse Generator.

Figure 26.   Oscilloscope.

THIS PAGE INTENTIONALLY LEFT BLANK

IV. EXPERIMENTAL PROCEDURE

The laser holder was assembled with the parabolic mirror, flat mirror, and laser. This assembly was mounted on the cold head of the cryogenic cooler. The resistance of the laser was measured using a Fluke multimeter and found to be about 7.2Ω at room temperature. The vacuum pump was activated to remove the air in the shroud and the cooler was started.

The cryogenic cooler requires at least two hours to cool the assembly down to 10K. The temperature sensor was monitored the entire time, and when it read 10K the resistance of the electrical circuit was again measured. This is necessary because the thermal sensor does not lie on top of the laser. Once the Fluke meter had stopped changing (resistance was a stable value of $0.1M\Omega$), the temperature at the laser was approximately 10K.

The microbolometer infrared camera was placed approximately six inches from the cold head window. Its germanium optics were removed and replaced with the picarin lens. The camera's RF output was connected to a computer using a framegrabber (Video Capture Essentials) to record the laser beam.

Next, the pulse generator and oscilloscope were activated. The pulse generator was checked to ensure the correct pulse parameters were set. The laser was pulsed with a square wave whose frequency was 100 kHz. The pulse width was 500 ns and duty cycle was 5%. The pulse had a negative slope (top contact to the laser being positive) and was driven between 100 mA to 1 A. It was observed that

the temperature of the cold head was increased from 10K to about 20K when the pulse generator was turned on. This was primarily due to the dissipation of about 10W of peak power or 0.5 W of average power during the operation. The output pulse settings are summarized in Table 1. The input current, output current, temperature, and images were recorded. Figure 27 depicts the overall equipment set-up.
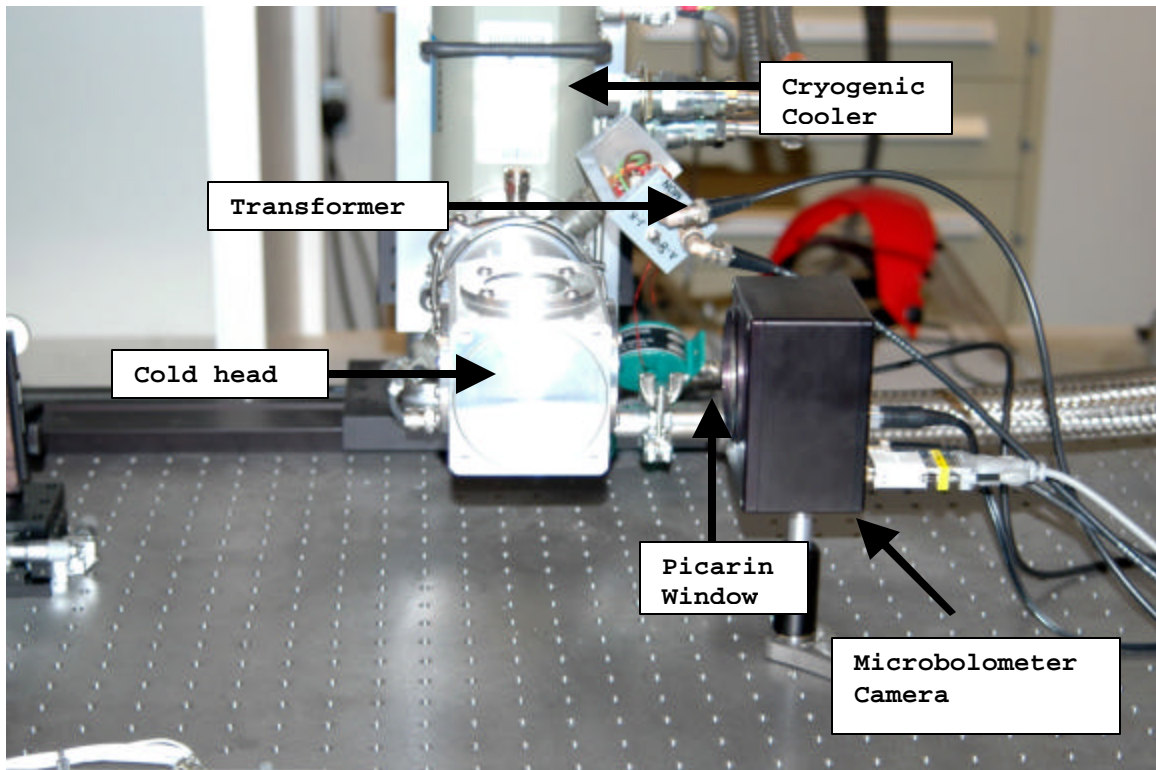
Figure 27.   Experiment set-up.

Frequency	Period	Delay	Duty Cycle	Width	Amplitude	Pulse Slope
100*kHz*	10**ms**	0*ns*	5%	500*ns*	Current- 200*mA*	Negative

Table 1.   Pulse generator output settings.

V. RESULTS AND RECOMMENDATIONS

A. CURRENT AND SIGNAL OUTPUT

The input signal described in Chapter IV ran from the power generator through the step-down transformer. The current through the laser and output voltage of the transformer were both monitored and recorded and are shown in Figures 28 and 29, respectively.
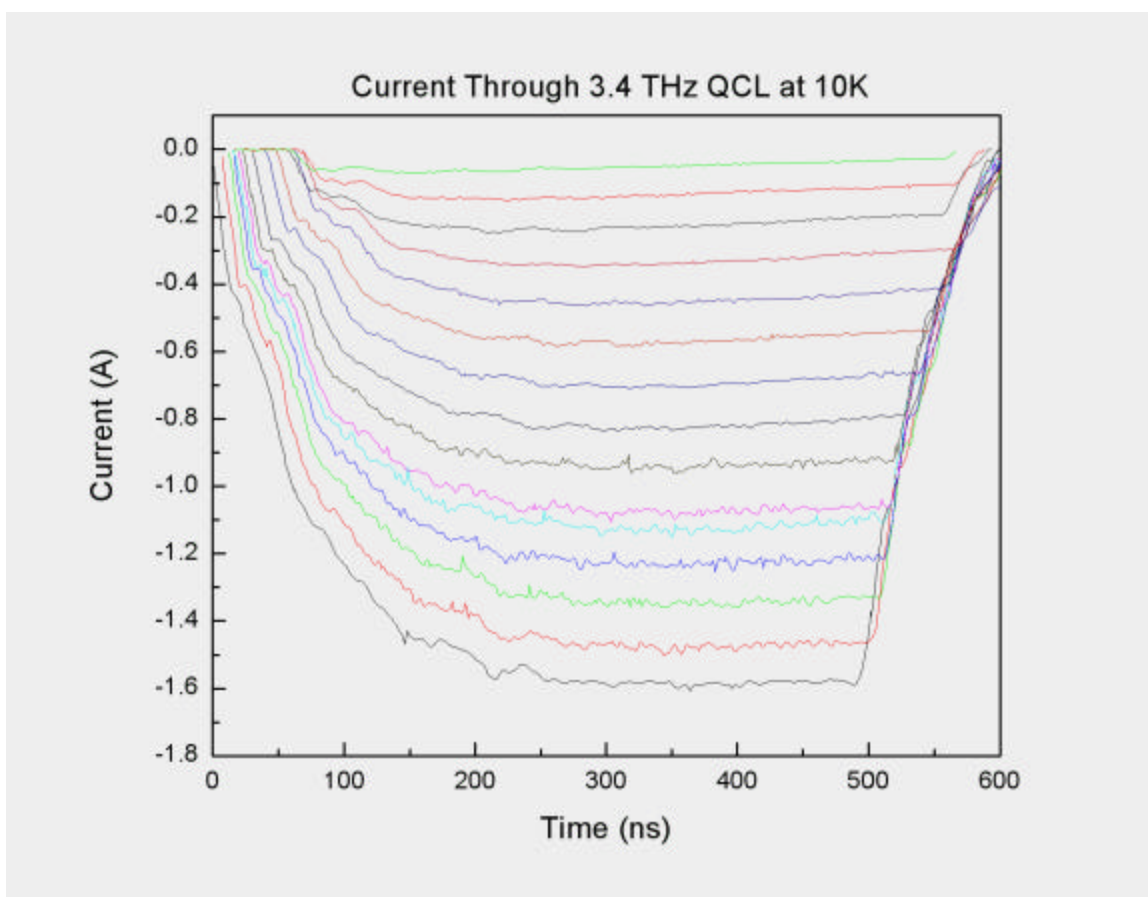
Figure 28.   Current as a function of time in steps of 50 mA through laser.
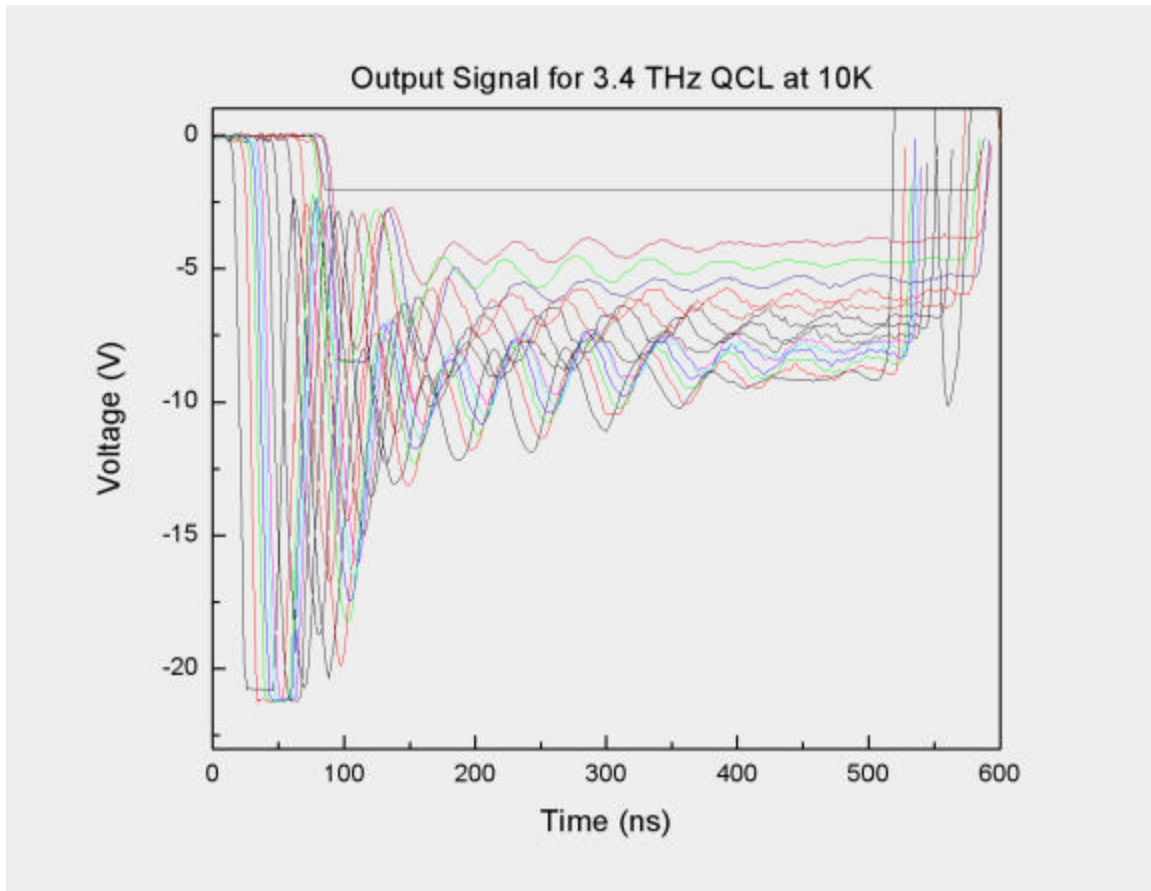
Figure 29.   Voltage across the output of the
                        transformer.

It can be seen that the output voltage oscillates at
the edges of the pulse primarily due to the inductance of
the ferrite core, transformer coupled with the cable
capacitance and impedance of the pulse generator.   Further
refinement of the electrical circuit is needed to minimize
such ringing. However, a major portion of the pulse is
relatively flat.   The ringing was not seen in the current
traces in Figure 28 due to the integrating done with the
current monitor.   The data in Figures 28 and 29 were used
to generate the I-V characteristics of the laser at the
operating temperature of about 10K as depicted in Figure
30.

34
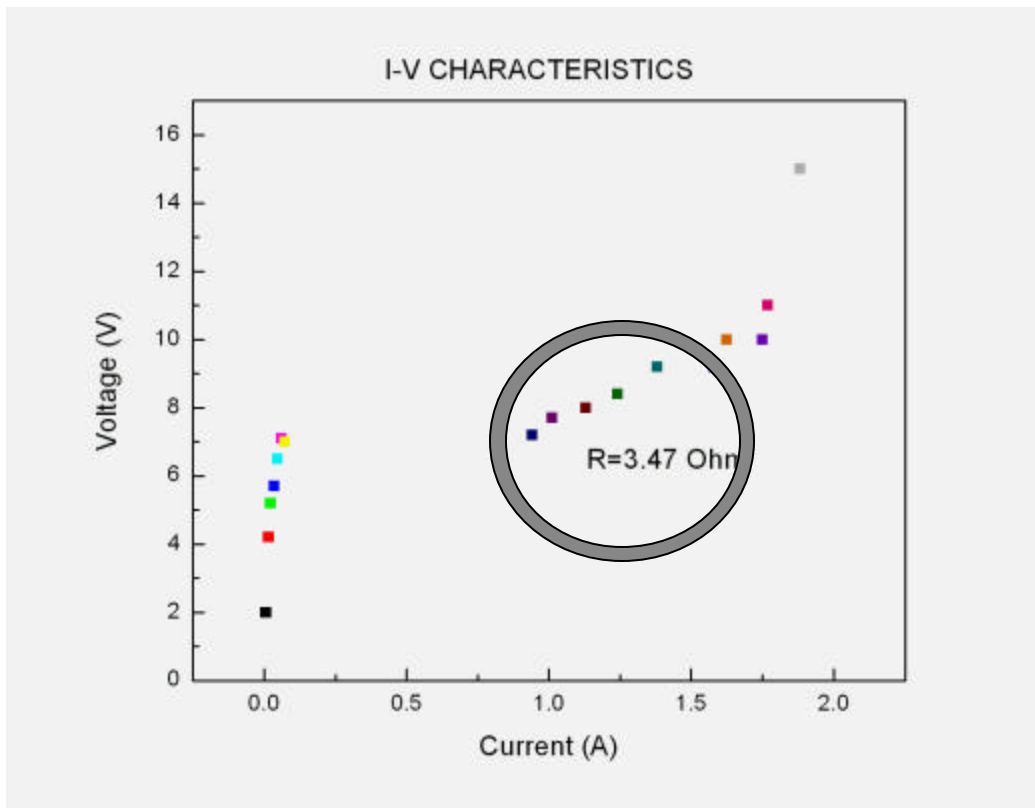
Figure 30.   I-V Characteristics for 3.4 THz laser for
        input current greater than 100 mA. The blue
     circle represents the current range over which
                  the laser lased.

B.   IMAGES OF LASER BEAM

The input electrical pulses of 1 A and 10 V along with a cryogenic cooler temperature of approximately 20K produced THz rays that were captured by the microbolometer. The following pictures were captured with Video Capture Essentials software.

1.5 A, 9 V   1.0 A, 7 V

750 mA, 6.5 V
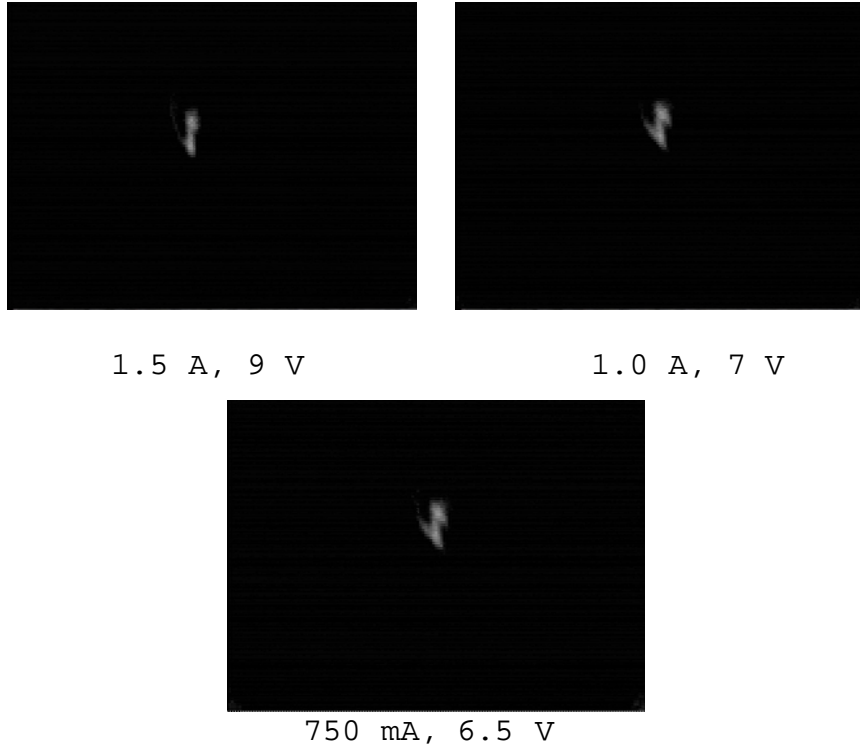
Figure 31.   Three images of THz radiation captured by
microbolometer.

The image of the THz beam is approximately 20mm x 5mm.
It is not circle in shape due to the multimode nature of
the laser emission.

It was observed that the laser power reduces with the
number of electrical pulses due to heating of the active
region of the laser. As mentioned before, the use of high
current and voltage pulses generate about 10 W of peak
power. In addition, the laser power is strongly dependent
on the pulse current as illustrated by the images in Figure
31. As expected, the THz light was transmitted through
clear plastics (see Figure 32).
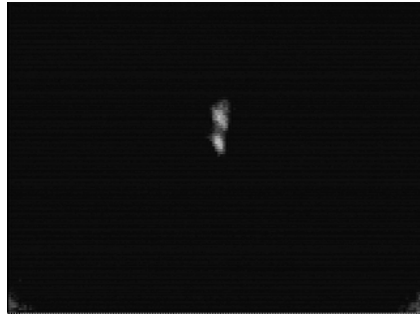
Figure 32.   Clear plastic in front of THz beam at 1.2 A,
7.5 V.

In summary, during the course of this project a cryogenically cooled quantum cascade laser operating in THz frequencies was successfully implemented. The output of the laser was imaged using an uncooled microbolometer infrared camera fitted with a picarin lens, which has a good transmission in THz frequencies. The initial results indicate that such a setup can be used for real-time imaging in the THz spectrum.

C.   FUTURE WORK RECOMMENDATIONS

The following are recommendations for future work in the field of terahertz imaging using a QCL and uncooled microbolometer camera.

It is easily demonstrated that the beam output power decays with the increase in temperature at the lasing site. In order to have a stronger signal sent to the camera, the output power of the QCL must be enhanced. One recommendation is to place a cold shield around the laser inside the vacuum shroud. More research needs to be completed in this area to maximize the removal of heat generated by the laser during the operation.

The second recommendation for future work is to optimize the light collection optics. The beam output is not perfectly collimated. Work on correcting this involves the use of a thinner flat mirror or modification of the flat mirror holder to improve the collimation.

Finally, research into characterizing the microbolometer camera's operation in other THz wavelengths needs to be completed. The NETD analysis was started in Chapter III but needs to be completed. The ultimate goal of research in this field is to design an uncooled microbolometer for THz imaging that is portable, cheap, and effective. This last research recommendation is fundamental in achieving that goal.

APPENDIX A.

A. MATLAB PROGRAM FOR PLANCK BLACKBODY RADIATION LAW APPROXIMATION

```
nu=1e12:1e10:10e12
k=1.38e-23
T=300
c=3e8
h=6.63e-34
dnu=1e12

p=(2*pi*k*T*nu.^2)/(c*c);

figure (1), clf
plot (nu,p)
axis([1e12 5e12 0 5e-12])
xlabel ('Frequency (Hertz)')
ylabel ('Power (Watts)')
title ('Power Emitted Per Unit Area Per Unit Frequency Interval')
```

B. MATLAB PROGRAM FOR PLANCK BLACKBODY RADIATION LAW

```
nu=1e12:1e8:8e13
h=6.63E-34
k=1.38E-23
T=300
c=3E8
dnu=1e8

A=((2*pi*h).*nu.^3)./(c*c)
B=(exp((h.*nu)./(k*T)))-1
p=A./B
D=sum(p)*dnu

figure (1)
plot (nu,p)
xlabel ('Frequency (Hertz)')
ylabel ('Power (Watts)')
title ('Power Emitted Per Unit Area Per Unit Frequency Interval')
```

C. MATLAB PROGRAM FOR COMPARISON OF EQUATION 2.1 AND EQUATION 2.4

```
h=6.63E-34
k=1.38E-23
c=3E8
dnu=1e9
nu=1e10:dnu:5e12
sigma=5.67e-8
for n=1:31
    T(n)=90+10*n
    A=((2*pi*h).*nu.^3)./(c*c)
    B=(exp((h.*nu)./(k*T(n))))-1
    p=1e-4*(A./B)
    D(n)=sum(p)*dnu
end

D2=(2*pi*k*T*5e12^3*1e-4)/(3*c*c)

figure (1)
hold on
plot (T,D)
plot (T,D2,'—')
axis([100 400 0 1.8E-3])
xlabel ('Temperature (K)')
ylabel ('Power (W/cm^2)')
title ('P(T)')
hold off
```

THIS PAGE INTENTIONALLY LEFT BLANK

APPENDIX B.

A. PROCEDURE FOR OBTAINING CORRECT TURN RATIO ON TRANSFORMER

   The transformer used contained five wires wrapped around a toroid. The turn ratio of all possible combinations was found by measuring the input and output voltages (in mV). Using the relationships in equations 3.8 and 3.9, the voltage is related to the turn ration. From there the number is squared. This is the desired number. Table 2 lists the data taken.

Wire (out)	Wire (in)	$V_{out}/V_{in} = N_{out}/N_{in}$	Squared Number
1	2	100/40=2.5	6.25
1	3	100/40=2.5	6.25
1	4	100/40=2.5	6.25
1	5	200/170=1.18	1.38
2	1	250/100=2.5	6.25
2	3	1	1
2	4	1	1
2	5	90/170=0.53	0.28
3	1	250/100=2.5	6.25
3	2	1	1
3	4	1	1
3	5	81/170=0.476	0.23
4	1	100/260=0.385	0.148

Wire (out)	Wire (in)	$V_{out}/V_{in} = N_{out}/N_{in}$	Squared Number
4	2	1	1
4	3	1	1
4	5	90/173=0.52	0.27
5	1	210/260=0.808	0.65
5	2	82/41=2	4
5	3	78/37=2.1	4.44
5	4	81/40=2	4

Table 2.   Transformer Data to determine squared turn ratio.

Applying the data from Table 2, wires four and five were kept on the transformer and all others were removed.

LIST OF REFERENCES

1. J.E. Bjarnason, L.J. Chan, W.M. Lee, M.A. Celis, & E.R. Brown "Millimeter-wave, terahertz, and midinfrared transmission through common clothing," *Appl. Phys. Lett.* 85 519 (2004).

2. D.A. Zimdars, & J.S. White, "Terahertz reflection imaging for package and personnel inspection," *Proc. SPIE* 5411 78 (2004).

3. J. O'Hara,& D. Grischkowsky, "Synthetic phased-array terahertz imaging," *Opt. Lett.* 27 1070 (2002).

4. R.H. Clothier, & N. Bourne, "Effects of THz exposure on human primary keratinocyte differentiation and viability," *J. Biol. Phys* 29 179-85 (2003).

5. J.F. Federici, B. Schulkin, F. Huang, D. Gary, R. Barat, & F. Oliveira, "THz imaging and sensing for security applications-explosives, weapons and drugs," *Semiconductor Science and Technology, 20* 7 S266-S280 (2005).

6. F. De Lucia, "Noise, detectors, and submillimeter-terahertz system performance in nonambient environments," *Opt. Soc. Am. B*, 21 7 (2004)

7. Lawrence Berkeley National Laboratory (n.d.). *Filling the Terahertz Gap*. Retrieved 16 November 2006 from http://circe.lbl.gov/THzGap.html .

8. M.S. Shur, & V. Ryzhii, "New concepts for submillimeter-wave detection and generation," *Proc. 11th GaAs Symp.* 301-304 (2003).

9. K.A. McIntosh, E.R. Brown, K.B. Nichols, O.B. McMahon, W.F. DiNatale, & T.M. Lyszczarz, "Terahertz photomixing with diode lasers in low-temperature-grown GaAs," *Appl. Phys. Lett,* 67 3844 (1995).

10. G.L. Carr, M.C. Martin, W.R. McKinney, K. Jordan, G.R. Neil, & G.P. Williams, "High-power terahertz radiation from relativistic electrons," *Nature,* 420 153-156 (2002).

11. A.J. Miller, A. Luukanen, & E.N. Grossman, "Terahertz active direct detection imagers," *Proc. SPIE -Int. Soc. Opt. Eng,* (2004).

12. P.W. Kruse, *Uncooled Thermal Imaging: Arrays, Systems, and Applications.* Bellingham, Washington: SPIE (2002).

13. F.L. Pedrotti, & L.S. Pedrotti, *Introduction to Optics.* Saddle River, New Jersey: Prentice Hall (2003).

14. R.A. Wood, Monolithic silicon microbolometer arrays. *Uncooled Infrared Imaging Arrays and Systems, Semiconductors and Semimetals.* 47. San Diego, California: Academic Press (1997).

15. Infrared Solutions INC. IR-160 Thermal Imager product information sheet (2004).

16. Mesoscopic Physics Group (2003). *Quantum Cascade Laser.* Retrieved on 15 November 2006 from http://www.unine.ch/phys/meso/General/QCL/QC_laser.htm.

17. J. Faist, F. Capasso, D.L. Sivco, C. Sirtori, A.L. Hutchinson, & A.Y. Cho, "Quantum Cascade Laser," *Science*, *New Series*, 264 5158 553-556 (1994).

18. J. Faist, L. Ajili, G. Scalari, M., Giovannini, M. Beck, M. Rochat, H. Beere, A.G. Davies, E.H. Linfield, & D. Ritchie, "Terahertz Quantum Cascade Lasers," *Phil. Trans. R. Soc. Lond.,* 362 215-231 (2003).

19. D.J. Paul, University of Cambridge (2006). *Si/SiGe Quantum Cascade Lasers.* Retrieved 19 November 2006 from http://www.sp.phy.cam.ac.uk/~SiGe/QCL.html.

20. Agilent Laboratories (January 2004). *Imaging at 3.4 THz with a Quantum Cascade Laser* from PowerPoint presentation.

21. CTI-Cryogenics Helix Technology Corporation Users Manual for Model 22C/350C Cryodyne Refrigerators (1995). *Multiple Uses of Model 22C/350C Cryodyne Refrigerators: Installation, Operation, and Servicing Instructions.* Mansfield, Massachusetts: CTI Cyrogenics-Helix Technology Corporation.

22. MicroTech Instruments, INC (n.d.). *Transmission Spectra of Picarin and Polyethylene*. Retrieved 19 October 2006 from http://www.mtinstruments.com/thzlenses/index.htm.

23. Pearson Electrons (n.d.). Retrieved October 2006 from http://www.pearsonelectronics.com/current-monitor-products/application-notes.htm.

24. P. Helisto (2006). *Development of a High-Resolution THz Scanner Based on Superconducting Microbolometers and Room Temperature Readout.* Presented during the SURA Terahertz Applications Symposium on Friday, June 2, 2006 in Washington D.C.

THIS PAGE INTENTIONALLY LEFT BLANK

INITIAL DISTRIBUTION LIST

1. Defense Technical Information Center
    Ft. Belvoir, Virginia

2. Dudley Knox Library
    Naval Postgraduate School
    Monterey, California

3. Professor Gamani Karunasiri
    Naval Postgraduate School
    Monterey, California

4. Professor Nancy Haegel
    Naval Postgraduate School
    Monterey, California

5. Professor James Luscombe
    Naval Postgraduate School
    Monterey, California